JCI insight

MiR-*16* regulates crosstalk in NF-kB tolerogenic inflammatory signaling between myeloma cells and bone marrow macrophages

Jihane Khalife, … , Enrico Caserta, Flavia Pichiorri

JCI Insight. 2019. https://doi.org/10.1172/jci.insight.129348.

Research In-Press Preview **Hematology** **Oncology**

High levels of circulating miR-*16* in the serum of multiple myeloma (MM) patients are independently associated with longer survival. Although the tumor suppressor function of intracellular miR-*16* in cancer cells, including MM plasma cells (PCs), has been highly elucidated, its extracellular role in maintaining a non-supportive cancer microenvironment has not been fully explored. Here, we show that miR-*16* can be actively secreted by MM cells through extracellular vesicles (EVs), and its extracellular and intracellular levels are directly correlated. We also show that EVs isolated from MM patients and from the conditioned media of MM-PCs can differentiate circulating monocytes to M2-tumor supportive macrophages (TAMs) and that the presence of higher levels of extracellular miR-*16* counteracts this effect. In agreement with these observations, our data show that miR-16 directly targets the IKKα/β complex of the NF-kB canonical pathway, which is known to play a critical role in polarizing macrophages toward an M2 phenotype. By using a miR-*15a-16-1* knockout mouse model, we also show that loss of the miR-*16* cluster supports polarization to M2-macrophages. Finally, we demonstrate the therapeutic benefit of miR-*16* overexpression in potentiating the anti-MM activity by a proteasome inhibitor in the presence of MM resident bone marrow TAM.

MiR-*16* regulates crosstalk in NF-κB tolerogenic inflammatory signaling between myeloma cells and bone marrow macrophages

Jihane Khalife[1,2]*, Jayeeta Ghose[3]*, Marianna Martella[1,2], Domenico Viola[1,2], Alberto Rocci[4], Estelle Troadec[1,2], Cesar Terrazas[5], Abhay R Satoskar[5], Emine Gulsen Gunes[1], Ada Dona[1], James F Sanchez[1], P Leif Bergsagel[6], Marta Chesi[6], Alex Pozhitkov[7], Steven Rosen[1], Guido Marcucci[2,8], Jonathan J Keats[1,9], Craig C Hofmeister[10], Amrita Krishnan[1], Enrico Caserta[#1,2] and Flavia Pichiorri[#1,2]

1. Judy and Bernard Briskin Center for Multiple Myeloma Research, City of Hope, Duarte, CA, USA
2. Department of Hematologic Malignancies Translational Science, City of Hope, Duarte, CA, USA
3. Department of Radiation Oncology, The Ohio State University, Columbus, OH, USA
4. Faculty of Biology, Medicine and Health, School of Medical Science, Division of Cancer Science, University of Manchester, Manchester, United Kingdom
5. Division of Experimental Pathology, Department of Microbiology, The Ohio State University Medical Center, Columbus, OH, USA
6. Department of Medicine, Mayo Clinic Arizona, Scottsdale, AZ, USA
7. Department of Computational and Quantitative Medicine, City of Hope, Duarte, CA, USA
8. Gehr Family Center for Leukemia Research, City of Hope, Duarte, CA, USA
9. Translational Genomics Research Institute, Phoenix, AZ, USA
10. Department of Hematology and Medical Oncology, Emory University School of Medicine, Atlanta, GA, USA

* These authors contributed equally to the work

Corresponding authors:

Flavia Pichiorri, 1500 E Duarte Rd, Duarte, CA, 91010 USA Phone: 626-218-4908
Email: fpichiorri@coh.org
Enrico Caserta, 1500 E Duarte Rd, Duarte, CA, 91010 USA Phone: 626-218-8519
Email: ecaserta@coh.org

Conflict of interest statement: The authors have declared that no conflict of interest exists

Abstract

High levels of circulating miR-*16* in the serum of multiple myeloma (MM) patients are independently associated with longer survival. Although the tumor suppressor function of intracellular miR-*16* in MM plasma cells (PCs) has been elucidated, its extracellular role in maintaining a non-supportive cancer microenvironment has not been fully explored. Here, we show that miR-*16* is abundantly released by MM cells through extracellular vesicles (EVs), and that differences in its intracellular expression as associated with chromosome 13 deletion (Del13) are correlated to extracellular miR-*16* levels. We also demonstrate that EVs isolated from MM patients and from the conditioned media of MM-PCs carrying Del13 more strongly differentiate circulating monocytes to M2-tumor supportive macrophages (TAMs), compared to MM-PCs without this chromosomal aberration. Mechanistically, our data show that miR-*16* directly targets the IKKα/β complex of the NF-κB canonical pathway, which is critical not only in supporting MM cell growth but also in polarizing macrophages toward an M2 phenotype. By using a miR-*15a-16-1* knockout mouse model, we found that loss of the miR-*16* cluster supports polarization to M2-macrophages. Finally, we demonstrate the therapeutic benefit of miR-*16* overexpression in potentiating the anti-MM activity by a proteasome inhibitor in the presence of MM resident bone marrow TAM.

Introduction

Multiple myeloma (MM) is the second most frequent blood cancer in the USA after non-Hodgkin lymphoma (1) and is characterized by the accumulation of over 10% of plasma cells (PCs) in the bone marrow (BM) (2, 3). In all cases, MM is preceded by a premalignant disease known as monoclonal gammopathy of undetermined significance (MGUS) (4-7), and, independently of specific genetic and epigenetic changes, all PCs at the beginning of the disease are dependent on the BM niche (8), which plays a pivotal role in the regulation of their growth, survival and eventual drug resistance (9, 10). Of all the different essential survival signals activated in PCs by external BM stimulations, the *NF*-κB pathway and subsequent production of supportive growth factors (e.g., IL-6, IL-8, TNF-alpha and VEGF) and adhesion molecules including (CD44, CD184, and ICAM-1) play a central role in PC proliferation and survival and subsequent drug resistance and/or resistance to standard-of-care proteasome inhibitors (PIs) (11). NF-κB constitutive activity is found in the cancer cells of MGUS and MM patients (12), and although the presence of promiscuous genetic mutations in the NF-κB pathway can explain NF-κB activation in a subset of MM patients (20%) (13), it cannot account for the majority of the MM cases with no genetic abnormalities (12, 14). The long arm of chromosome 13 (13q) is variably deleted (Del. 13) in regions, which includes deletions in the region of the *miR-16-15a* cluster (15). Del(13) occurs in almost 50% of newly diagnosed MM patients (16) and can reach up to 80% in patients with active disease (17), but it is also present at lower percentages in patients with MGUS (18). However, Del(13) was seen to be correlated with the transformation of MGUS to MM, and it is found at much higher frequency in patients with high-risk features such as t(4;14) (88%) and MAF (73%) translocations (19), highlighting that progression of chromosome 13 abnormalities requires clonal evolution (20). The *miR-15a-16-1* cluster is located in the intronic region of the Deleted in Lymphocytic Leukemia 2 (DLEU2) gene coding for mature miRNAs (i.e., miR-*15a* and -*16-1*), which has been shown to regulate the expression of pivotal oncogenes in cancer initiation and

progression, including BCL-2, MCL-1, and cyclin D (21-23). Recently, the possible role of this class of miRNAs in regulating not only the cancer cell intracellular landscape but also the tumor microenvironment by their secretion through extracellular vesicles (EVs) has been proposed (24, 25). We previously showed that extracellular miR-*16* is among the few microRNAs that can be used as a prognostic biomarker in newly diagnosed MM patients treated with proteasome inhibitor-based therapy (26). Previous studies have shown the role of endogenous miR-*16* in shifting macrophage (MΦ) polarization from a tumorigenic (tumor supportive M2) to tumoricidal (anti-tumor M1) phenotype (27). Recently published data have revealed that in MM, tumor associated macrophages (TAMs) are recruited into the BM and protect cancer cells from chemotherapy-based apoptosis (28), and increased levels of BM TAM in MM patients are associated with poor prognosis (29).

In this study, we investigate the possible consequences of loss of miR-*16* associated with Del. 13 in supporting PC degeneration during disease development. Specifically, we explore whether loss of miR-*16* in the PCs can affect their fitness not only by changing the oncogenic landscape intracellularly but also by affecting the tumor microenvironment.

Results

Extracellular vesicles and intracellular miR-*16* levels are correlated

We previously reported that extracellular levels of miR-*16* were significantly downregulated (p=0.003) in the serum of MM patients carrying Del(13) in their MM cells compared to levels in patients in which Del(13) was not present (26), supporting the idea that extracellular miR-*16* levels may reflect the levels of miR-*16* in cancer cells. We then performed microRNA (miRNA) profiling of 4 different Del(13) MM cell lines (RPMI-8226, U266, MM.1R, NCI-H929) and their derived EVs (Figure 1A, Supplemental Table 1). miRNA analysis by Nanostring technology showed that miR-*16* was more enriched in the EVs compared to its endogenous levels (Figure 1B). Conversely, the same magnitude of EV enrichment was not found for other miRNAs including the highly endogenously expressed miR-*142-3p* (Figure 1B-C), as well as miR-*9*, the highly expressed and well-known cancer-associated biomarker released in EVs (Figure 1C) (30, 31). EV-miR-*16* enrichment was not only observed in MM cells but, as expected, was also observed in the EV isolated from healthy bone marrow stromal cells (Figure 1D), aligning with previously published data that showed that miR-15a is highly released by normal stromal cells (24). We then decided to investigate whether differences in chromosome 13 status could reflect changes in miR-*16* extracellular enrichment, as supported by our previous published study of MM patients (26). As expected, MM cell lines carrying Del(13) (OPM2, LP-1, L363, U266, MM.1S, NCI-H929, RPMI-8226) have lower extracellular miR-*16* compared to that in the few MM cell lines carrying both 13q alleles (WT) (OCIMY-5, OCI-MY1, MMM.1) (https://www.keatslab.org/) (Figure 1E).

miR-*16* is downregulated in the bone marrow macrophages (BM-MΦ) of MM patients.

Because miR-*16* has been shown to exert its anti-MM activity in the context of the BM microenvironment (BM-ME) (32), and since PCs at the beginning of the disease rely on exocrine IL-6 production from the BM-ME for their survival (33), we investigated which cellular population

is the main IL-6 producer in this setting. Cytokine arrays show that the BM CD14+ positive fractions from MM patients, which we found to be mainly enriched in macrophages (CD14+/CD68+, BM-MΦ) (Supplemental Figure 1), are the main producers of NF-κB-dependent cytokines/chemokines including IL-6, IL-8, and TNF-α (Figure 2A), a group of cytokines that were significantly upregulated in the BM-MΦ of MM patients (n=4) as compared to those in cancer-free donors (n=4, HD) (Figure 2B).

We then asked whether this population could be affected by differential expression of EV miR-*16*. Our data show that miR-*16* is significantly downregulated in the MM-BM-MΦ (n=7 pts) compared to that isolated from healthy donors (n=7 pts) (Figure 2C). To unequivocally evaluate the downregulation of miR-*16* in the BM compartment of MM patients, we also compared the miR-*16* levels between MM BM-MΦ and their matched peripheral blood monocytes (PB-M) (n=3 patients). We found a significant decrease in miR-*16* expression in MM BM-MΦ as compared to their circulating fraction (Figure 2D).

To further assess whether miR-*16* down-modulation may be associated with monocyte to MΦ differentiation toward the M2-MΦ phenotype, we first induced differentiation of PB-M isolated from MM patients in vitro in the presence of the M2 differentiation factor M-CSF for 7 days. As expected, upon M-CSF treatment, the cells appeared more filamentous, having an endothelial-like shape indicative of the M2 phenotype, as compared to the control untreated undifferentiated (UI) cells (Figure 2E). A GFP-fluorescence latex beads-phagocytosis assay showed that cells treated with M-CSF were fully differentiated (84% GFP+) as compared to UI cells (4.63% GFP+) (Figure 2F) and showed significant increases in the mRNA of typical M2-MΦ expression markers including CD163 and IRF4 (Figure 2G-H). We also observed that M2-MΦ had a significant decrease in miR-*16* expression upon differentiation (Figure 2I). In summary, our findings show

that miR-*16* is down-modulated in the MM BM-MΦ and its downregulation in vitro is associated with an M2-MΦ phenotype.

Extracellular miR-*16* impairs MM-EV-induced M2-MΦ

Because previously published data have shown that, by producing soluble factors, MM cells can modify the BM niche and induce MΦ polarization toward an M2 tumor-supportive phenotype (34), we investigated whether the BM acellular fraction (BM-ac), the soluble portion of the BM, of MM patients could directly affect MΦ differentiation. We found that monocytes isolated from MM patients (MM-PB-M) tend to differentiate to an M2-like MΦ when treated with their matched BM-ac for 7 days (Figure 3A). Specifically, we observed that, after 7 days of incubation, the shape of PB-M was filamentous and appeared similar to those differentiated with M-CSF (Figure 3A, Figure 2E). miR-*16* expression was markedly downregulated in the PB-M differentiated with the BM-ac fraction compared to that in the matched undifferentiated PB-M. miR-*16* levels upon in vitro differentiation were fully comparable to those in MM-BM MΦ isolated from the same patient (Figure 3B). We then sought to identity the component in the BM-ac that was responsible for inducing an M2-like phenotype. Our data show that EVs isolated from the BM-ac of four MM patients induced differentiation of PB-M isolated from healthy donors to M2-MΦ (n=4), whereas no differentiation was observed when cells were incubated with the EV-depleted fractions (Figure 3C, Supplemental Figure 2A). Our data show that these differentiated cells are effectively MΦ, as they engulfed and digested fluorescent latex beads as demonstrated by a phagocytosis assay (Figure 3D). Interestingly, PB-M did not show any differentiation towards an M2 phenotype as assessed by the M2 markers CD163 and CD206 when treated with the conditioned media of the cultured total BM cellular population isolated from three cancer-free donors (BM-HD) as compared to those isolated from MM patients. In fact, almost all of the cells were dead after 7 days of treatment with the conditioned media of BM-HD (Supplemental Figure 2B). To assess whether

the EVs produced by MM cells are directly responsible for driving PB-M differentiation to M2-MΦ, we isolated EVs from the conditioned media of Del(13) MM cells (NCI-H929 and MM.1S). We found that healthy PB-M treated with MM-derived EVs for 7 days tend to differentiate toward an M2 phenotype, as shown by the increased expression of the M2 marker CD163 (Figure 3E). We have previously shown that newly diagnosed MM patients with Del13 have lower circulating miR-*16* levels compared to those in patients with non-Del13 (26), and other groups have found that increased levels of the EV miR-*15a* (miR-*15a/16-1* cluster) can inhibit MM cell growth (24). We then decided to investigate whether high levels of ectopic extracellular miR-*16* can impair monocyte to M2-MΦ differentiation. When PB-M isolated from healthy donors were treated with EVs isolated from the conditioned media of either MM.1S or NCI-H929 and concomitantly incubated with a double-stranded miR-*16* mimic encapsulated in lipid rafts (ds-miR-*16*), we observed lower CD163 surface expression as compared to that in PB-M treated with EVs in the presence of double-stranded miR-223 mimic (EV+miR-*223*) or Scramble *(*EV+Scr) (Figure 3F, Supplemental Figure 2C). Interestingly, a higher increase in CD163 levels was observed for both undifferentiated and differentiated PB-M when treated with a miR-*223* mimic, a miRNA that is known to be implicated in maintaining MΦ in an M2-like phenotype (Figure 3F, Supplemental Figure 2C) (35). In support of these data, the EV-treated monocytes appeared less filamentous, and few or no detectable endothelial-shaped cells were present upon treatment with ds-miR-*16,* in contrast to that from scramble sequences (Figure 3G, Supplemental Figure 2D). Taken together, our data show a functional effect of miR-*16* in impairing M2-MΦ differentiation.

EV isolated from MM cells carrying Del(13) strongly induce MΦ polarization

Because we showed that high levels of ectopic extracellular miR-*16* impair monocyte to MM-EV-driven M2-MΦ differentiation, we decided to investigate whether differences in miR-*16* EV enrichment could differentially impact this effect. We isolated EV from MM cells carrying either a

well-characterized Del(13) (OPM2, LP-1, L363) or intact wild type alleles (OCIMY-5, OCI-MY1, MMM.1). These EVs were found to express different miR-*16* copy numbers (Figure 1E). In agreement with our data, we found that EVs isolated from Del(13) cell lines induced significantly higher levels of MΦ differentiation to an M2-like phenotype compared to EVs isolated from cells carrying the wild type allele, as assessed by levels of M2 markers such as the mannose receptor (CD206) and CD163 as early as 4 days of PB-M treatment using the same primary CD14+ cells across cell lines ($p<0.01$) (Figure 4A-C). We then investigated whether EVs from patients carrying Del(13) could also induce monocyte differentiation. We found that the BM acellular fraction isolated from patients carrying Del(13) significantly induced more PB-M differentiation towards an M2 like phenotype as compared to that from patients carrying the wild type form (n=3/group) (Figure 4D-F).

Evaluation of MΦ polarization in a miR-*15a*/*16-1* knockout model

To further examine the in vivo effects of miR-*16* on MΦ polarization, we used a miR-*15a*/*16-1* knockout mouse model that was thoroughly established by Klein et al (21), which resembles the human miR-*15a*/*16-1* cluster deletion by carrying the corresponding alteration on mouse chromosome 14qC3. Since markers of differentiation were not observed at basal levels (data not shown, (27)), primary basal state spleen MΦ (M0-MΦ) (Supplemental Figure 3A) were isolated from miR-*15a*/*16-1* null or wild type B6 mice and induced to differentiate to M2-like cells following M-CSF and IL-4 treatment ex vivo (27). In response to IL-4 treatment, M0-MΦ isolated from miR-*15a*/*16-1* null mice presented a significantly more pronounced M2 phenotype compared to that in the wild type mice, as measured by the expression of mouse M2 markers such as CD206 and C-type lectin (Dectin-1) at an early (48 hr) (Figure 5A,E) or late (6 days) differentiation time (Figure 5B,F). As early as 48 hrs, miR-*15a*/*16-1* null MΦ expressed an average of a 10-fold increase (6.25 ± 1.6%) in CD206 (Figure 5 A,C) and an almost 5-fold increase (23.5 ±8%) in Dectin-1 (Figure 5

E,G) as compared to levels from wild type mice, which were 0.6±0.4% and 4.9%±0.7%, respectively (p= 0.001, CD206; p=0.008, Dectin-1; n=4/group). Isotype controls for each panel of the MΦ population at respective time points of 2 days (Figure 5A,E) and 6 days (Figure 5B,F) were given. miR-*15a*/*16-1* null M0-MΦ differentiated to M2-MΦ also show significant mRNA deregulation of M2-effector functional markers such as $IL10^{high}$ and $IL12^{low}$ (Supplemental Figure 3 B-C).

MiR-*16* directly regulates the expression of IKKα/β complex

We have shown that cytokines and growth factors, direct targets of the NF-κB canonical pathway which is dependent on the IKKα/β kinase complex (36), are the main players secreted by MM BM-MΦ. Previous studies have also shown that the canonical (classical) NF-κB pathway is an important regulator of the TAM transcriptional program (37), whereas the non-canonical pathway is mainly involved in immune cell differentiation and organogenesis (38). We then proceeded to investigate whether ectopic expression of miR-*16* could regulate the IKK complex in primary samples. Our data show that when MΦ isolated from MM patients were treated with ds-miR-*16*, the expression levels of both IKKα and β were significantly down-modulated, in contrast to treatment with Scr control (Figure 6A). The same effect was seen when a macrophage-like malignant cell line, U-937, or a human stromal cell line, HS-5, were transfected with ds-miR-*16* (Figure 6B-C)**.** We also found that MΦ isolated from miR-*15a/16-1* knockout mice had significantly higher endogenous IKKα/β expression levels as compared to wild type MΦ both at the protein and mRNA levels (Figure 6D-F, Supplemental Figure 4A). Interestingly, given the importance of the IKKβ subunit in signaling the NF-κB canonical pathway (36), differentiation of PB-M to M2-like MΦ using M-CSF showed significantly higher expression of IKKβ as compared to cells differentiated to M1-like MΦ (Supplemental Figure 4B). NF-κB pathway activation is not only associated with the production of MM supportive cytokine/chemokines by the BM

microenvironment but is also involved in MM cell autologous survival and proliferation (14). Because Del13 containing the miR-*15a*/*16-1* cluster (15) is observed in a high percentage of MM patients (17), we assessed whether MM-PCs carrying this genetic abnormality could show significant changes in the mRNA expression of the IKK complex. Using the MMRF CoMMpass IA13 dataset, we modelled the occurrence of Del13 [1/0] as a function of sex [1/2], age, 13q14 deletion [1/0], and expressions of ENSG00000213341 (IKKA), ENSG00000104365 (IKKB), ENSG00000231607 (DLEU2), and ENSG00000075624 (ACTB). The gene ACTB (actin) was chosen as a housekeeping gene not expected to be correlated to the Del13. We found a significant increase in IKKα mRNA expression (model coefficient=0.13, $p<0.001$) in the MM-PCs isolated from 355 newly diagnosed patients carrying Del13, compared to levels in 330 patients without this aberration. As expected, a strong correlation between the presence of Del(13) and a decrease in miR-*15a*/*16-1* host gene (DLEU2) mRNA expression in CD138+MM cells carrying Del(13) was also observed (model coefficient=-0.08, $p<0.001$). In support of these data, miR-*16* ectopic expression inhibited IKK complex expression in multiple MM cell lines (MM.1S, NCI-H929, U266), and this effect was not only restricted to IKKα but also to β (Figure 6G-H). Because we did not find significant upregulation of IKKβ at the mRNA level in MM-PCs with Del(13), we investigated whether this subunit could instead be regulated at the translational level or be a miR-*16* indirect target. By using TargetScan software prediction (39), we found a highly conserved microRNA responsive sequence (MRE) in the 3'UTR of IKKβ at position 603-610. To assess whether miR-*16* could affect IKKβ expression by directly binding its 3'UTR and subsequently affect protein translation, we cloned a specific region containing nucleotides 487-736 of the IKKβ 3'UTR that covers the predicted miR-*16* targeting sequence in a commercially available luciferase construct, pGL4.11. Luciferase reporter assays showed that miR-*16* significantly downregulated the activity of the reporter linked to IKKβ 3'UTR in U266 and HS-5 cell lines, compared to Scr control (Figure 6I). In support of IKKβ-specific miR-*16* targeting, a reporter vector carrying an IKKβ 3'UTR miR-*16* mutated seed sequence was not significantly affected by miR-*16* ectopic

expression (Supplemental Figure 4 C-D), supporting the idea that miR-*16* can directly regulate IKKβ. Taken together, our data indicate that the mechanism of action through which miR-*16* produces its effects is by directly targeting the IKKα/β complex.

MiR-*16* increases MM cell sensitivity to bortezomib by impairing the NF-κB signaling pathway

Because IKKα-IKKβ targeting (downregulation) may result in decreasing the degradation of the NF-κB inhibitor (IκBα) with subsequent inhibition of p65/p50 transcriptional activation (40), we investigated whether differential miR-*16* expression may regulate this process. Western blot data and single cell flow cytometry show that miR-*16* inhibits p65 translocation to the nucleus (Figure 7A-B). To determine whether miR-*16* inhibits NF-κB transcriptional activity, we performed transient assays using a reporter plasmid containing three tandem wild-type P65/P50-binding sites upstream of a luciferase gene. U-937 cells were transfected with the reporter, and NF-κB activation was induced by treatment with Tissue Plasminogen (TPA). We found that, whereas Scramble induced an almost three-fold change, miR-*16* induced a two-fold change in NF-κB binding activity (Figure 7C). Additionally, the same effect of miR-*16* was seen when ectopically expressed in HS-5, which is known to have a constitutively active NF-κB pathway (around 2-fold decrease in activity) (41) (Figure 7D). However, miR-*16* did not block the activity of a reporter containing three tandem mutated NF-κB sites, indicating that it specifically inhibits the canonical NF-κB pathway and that the inhibition does not block general transcriptional responses (Figure 7D). These results demonstrate that miR-*16* not only acts to inhibit the NF-κB signaling pathway but also the ability of NF-κB to activate gene expression in the bone marrow microenvironment (BM-ME), both in the MΦ compartment and stromal cells. As a result, miR-*16* significantly downregulated the release of NF-κB-dependent M2-like tumor promoting cytokines/chemokines,

IL-6, IL-8 and TNF-α, from BM-MΦ and upregulated the levels of IFN-γ (Figure 7E). IFN-γ has been previously shown to prevent the generation of TAM (42).

Because NF-κB is highly activated in MM cells (12), we tested the combinatorial effect of miR-*16* with a proteasome inhibitor (bortezomib) or the NF-κB inhibitor BAY11-7082 in MM cells. We found that ectopic expression of miR-*16* had a significant additive effect in inhibiting NF-κB transcriptional activity when MM cells where treated with bortezomib or BAY11-7082 (Figure 7F). At the molecular level, combination treatment of miR-*16* and bortezomib increased cytoplasmic levels of IκBα, the inhibitor of NF-κB, in three MM cell lines tested (MM.1S, NCI-H929 and RPMI-8226) after 8 hrs of treatment (Supplemental Figure 5A). To evaluate the clinical relevance of our findings, we examined whether miR-*16* can sensitize MM-PCs and/or resident MΦ of the BM microenvironment to bortezomib. We first examined the combinatorial effect of miR-*16* with low doses of bortezomib on an MM cell line, MM.1S, in vitro. We found that co-treatment of miR-*16* and bortezomib induced an additive decrease in cell viability in a dose-dependent manner (Supplemental Figure 5B). Ectopic expression of miR-*16* alone did not induce cell death in MM.1S, whereas in combination with low doses of bortezomib, miR-*16* sensitized MM cells to early apoptosis, as the combination treatment increased Annexin-V positive cells from 5.5% to 20%, in contrast to results from Scr control (Figure 7G). However, in the context of the BM microenvironment, it has been previously shown that M2 MΦ support MM cell survival and render them resistant to up to 5 nM bortezomib in culture (28, 43). Treatment of MM cells alone with low doses of bortezomib induced a decrease in cell viability, whereas in the presence of resident MΦ, the sensitivity was significantly abrogated (Figure 7H). For that reason, we investigated whether the combination treatment of miR-*16* and bortezomib would sensitize MM.1S to bortezomib in the presence of BM resident MΦ isolated from a MM patient. To specifically measure the viability of MM cells in co-culture systems, we used MM cells that constitutively express the luciferase gene (MM.1S GFP/Luc+), and we measured their viability by luciferase activity (Figure 7H-I). Co-

culturing GFP/Luc+ MM.1S with BM-MΦ showed that the presence of MΦ induced resistance of MM cells to cell death (Figure 7H). However, the attenuation of bortezomib-based anti-MM activity by MΦ was significantly reversed by ectopic overexpression of miR-*16* in both MΦ and MM cells (Figure 7I). Taken together, our results show that miR-*16* inhibits NF-κB transcriptional activity both in MM cells and the BM-ME and potentiates the activity of a proteasome inhibitor in a cross-talk manner by affecting both MM cells and BM resident MΦ.

Discussion

The BM-ME plays an important role in MM progression and response to therapy (9). MM cells interact with the BM-ME components in a paracrine manner, either by direct cell-cell interaction or indirect communication through release of soluble factors as well as EVs (44). Here we show that EVs released by MM cells induce monocyte differentiation towards an M2 phenotype. Our previous results showed that EVs released by MM cells are enriched in the MHC-1 antigen presenting complex and its binding protein, β2-M (26, 45, 46), and recent published data reported that this complex plays a pivotal role in inducing cancer cell protection from MΦ phagocytosis (47). Here we found that EVs isolated from MM patients' BM-ac fractions induce monocyte polarization towards an M2 phenotype. It has been reported that EVs derived from MM cells carrying miR-21 and miR-146a induce mesenchymal stromal cell proliferation and transformation, resulting in MM cell growth promotion and migration (48). We and others have shown that MM patients with high levels of circulating miR-*16* have longer survival and that circulating miR-*16* levels were reduced in the serum of MM patients carrying deletion 13 in their cancer cells as compared to levels associated with non-deletion 13 or normal PCs (26, 49), supporting that changes in chromosome 13 status may not only affect the intracellular landscape of cancer cells but also their tumor ME. Although a negative correlation between miR-*15a*/miR-*16-1* levels and the expression of the MM supportive cytokine IL-6 has been reported (24, 50), the molecular mechanisms behind this effect were not clearly investigated (50). We demonstrate that extracellular miR-*16* can impair the ability of MM EVs to differentiate monocytes to M2-MΦ and that ectopic expression of miR-*16* directly down-modulates NF-κB signaling. Specifically, we found that miR-*16* is not only able to target IKK-α as previously reported (51) but also the key catalytic kinase of the NF-κB canonical pathway, IKKβ, not only in MM cells but also in MΦ and BM stromal cells. We demonstrate that ectopic expression of miR-*16* impairs monocyte differentiation to M2-MΦ and the subsequent release of M2-associated cytokines/chemokines

such as IL-6, IL-10, IL-8 and TNF-α (Figure 8). We also show that Del(13), in addition to affecting the intracellular genetic landscape of MM cells as previously reported (16, 17), also impacts the surrounding BM-ME, creating a clonal advantage of cancer cells carrying this deletion versus the wild type form. The importance of miR-*16* in impairing M2-MΦ differentiation through IKKβ targeting is also supported by previously published data showing that the NF-κB canonical pathway alone is essential to maintain an M2 phenotype, as only the MΦ isolated from IKKβ knockout mice could be re-educated to have anti-tumor activity, in contrast to those isolated from WT mice (52). By using a miR-*15a*/*16-1* knockout mouse model (21), we also show that miR-*15a*/*16-1* knockout MΦ had a significantly stronger M2 phenotype as indicated by the M2 surface markers CD206 and Dectin-1, compared to that in wild type mice. These findings are also consistent with recently published data in which a miR*15-16* double knockout model exhibits myeloid disorders (53). Finally, we showed the clinical benefit of miR-*16* in sensitizing MM cells to bortezomib treatment. Our findings align with a clinical study that showed exosomal miR-*16* downregulation in patients with bortezomib resistance (54). We found that miR-*16* not only directly sensitized MM cells to bortezomib in an autologous manner but also reverted their PI resistance when myeloma cells were co-cultured in the presence of TAMs isolated from the BM aspirates of MM patients, further supporting that TAMs provide a survival benefit to MM cells (43). In summary, we show that EVs released by MM cells can affect the tumor ME by modulating the polarization of circulating monocytes to M2-MΦ, which fully resembled the BM-MΦ characteristics found in patients. Our data also show that miR-*16* can down-modulate the NF-κβ pathway in PCs and the microenvironment, in which activation is critical for maintaining MM-PC survival during early stage disease (14). Our data provide the scientific rationale for the manner in which miR-*16* down-modulation provides a survival advantage to specific PC clones during MM progression.

Methods

Primary Samples

Primary samples (total bone marrow aspirates and peripheral blood samples) from MM patients and healthy donors were obtained from The Ohio State University and City of Hope Leukemia Tissue Banks. Specifically, the cellular fraction of total bone marrow aspirates was isolated using Ficoll-Paque Plus (Cat.# 17144003,GE, Healthcare, Life Science) following the manufacturer's instructions.

Cell lines

MM cell lines (MM.1S, NCI-H929, U266 and RPMI-8226), the U-937 MΦ cell line, the BM stromal cell line HS-5, and the HeLa cell line were purchased from ATCC. The GFP+/Luciferase+ MM.1S stable line was a generous gift from Dr. Irene Ghobrial (Dana-Farber Cancer Institute). OPM2, LP-1, L363, OCIMY-I, OCIMY-5, and MMM.1 MM cell lines were provided by Dr. Jonathan J Keats (https://www.keatslab.org/). MM and U-937 cell lines were cultured in RPMI-1640 medium supplemented with 10% fetal bovine serum (Cat.#019K8420, Sigma), 100 IU/ml penicillin and 100 µg/ml streptomycin. The HS-5 cell line was cultured in DMEM supplemented with 10% fetal bovine serum, 100 IU/ml penicillin, and 100 µg/ml streptomycin. HeLa cells were cultured in EMEM supplemented with 10% fetal bovine serum, 100 IU/ml penicillin, and 100 µg/ml streptomycin.

Cell transfection

HS-5 or HeLa cell lines were transfected with Lipofectamine™ 3000 Transfection Reagent (Cat.#L3000-008, Invitrogen) following the manufacturer's instructions. MM cell lines were transfected by electroporation using the Nucleofector4D system (Lonza). Specific nucleofection solutions and programs were optimized for each cell line. Briefly, on day 1 two batches of $6x10^6$ cells were each resuspended in 100 µl of the nucleofector SF solution containing 50 pmol

microRNA hsa-miR-16-5p mimic (Thermo Fisher, Cat#4464066), or scramble control (Thermo Fisher, Cat#4464058) and transferred to a cuvette. Each electroporated batch of cells were then kept in culture in 10 ml complete growth media for the next day. On day 2, the two batches of cells were combined and transfected again following the same procedure. On day 3, cells were harvested for further experiments. Program DS-137 was used for MM.1S cells, program DN-100 for U266, program DS-150 for RPMI-8226, and program CM-138 for NCI-H929. All MM cell lines were transfected two times unless indicated otherwise in the figure legends. The U-937 cell line was transfected by electroporation using the Nucleofector4D system (Lonza) according to the manufacturer's instructions. Primary cells were transfected using DOTAP Liposomal Transfection Reagent (Cat#144189-73-1, Sigma-Aldrich) according to the manufacturer's instructions. The hsa-miR-223 mimic microRNA used was hsa-miR-223-5p mimic (Thermo Fisher, Cat#4464066).

mRNA and miRNA expression

Quantitative real time-PCR (qRT-PCR) was performed with the TaqMan method (Applied Biosystems), according to the manufacturer's instructions, and analyzed with the 7900HT Sequence Detection System (Applied Biosystems). The appropriate TaqMan probes for mRNA and miRNA quantification were purchased from Applied Biosystems, and all reactions were performed in triplicate. The following probes were used: hsa-miR-16-5p (477860_mir), hsa-miR-142-3p (000464_mir), hsa-miR-9 (000583_mir), hsa-CD163 (Hs00174705_m1), hsa-IRF4 (Hs00180031_m1), hsa-CD80 (Hs01045161_m1), hsa-IKKα (Hs00989497_m1), hsa-IKKβ (Hs01559460_m1), mm-IL-10 (Mm01288386_m1), mm-IL-12 (Mm00434169_m1), mm-IKKα (Mm00432529_m1), and mm-IKKβ (Mm01222247_m1). GAPDH (Hs99999905_m1) was used as a reference for human mRNA data normalization, while small endogenous nucleolar RNA RNU44 (001094) was used for miRNA normalization. Simultaneous quantification of ornithine decarboxylase antizyme 1 (OAZ1) (Mm00814770_g1) was used as a reference for mouse mRNA data normalization. The relative expression levels were calculated by the comparative cycle

threshold (Ct) method (User Bulletin#2; Applied Biosystems). EV-miRNA isolation for qRT-PCR analysis was done using the exoEasy Maxi Kit (Cat# 76064, QIAGEN, Valenica, CA) according to the manufacturer's instructions.

Monocyte differentiation

CD14+ cell isolation from primary samples, either bone marrow or peripheral blood, was done using CD14 microbeads (Cat# 130-050-201 Miltenyi Biotech, Bergisch Gladbach, Germany) according to the manufacturer's instructions. Isolated cells were differentiated for 7 days with granulocyte macrophage colony stimulating factor (GM-CSF) (20 ng/ml) or macrophage colony stimulating factor (M-CSF) (20 ng/ml) added every two days to generate in vitro M1 or M2-MΦ, respectively. Differentiation of CD14+ cells using EV isolated from MM cells was done at a ratio of 1 to 8 in culture for the time indicated in the figure legends. Differentiation of CD14+ cells with the BM-ac fractions or BM conditioned media was done at the ratio of $1x10^6$ CD14+ cells to 1 ml of BM-ac fractions in culture for the times indicated in the figure legends. Formally, we categorized the bone marrow acellular fraction (BM-ac) as the human bone marrow plasma, which mainly consists of dissolved proteins (chemokines, cytokines, growth factors etc), hormones, carbon dioxide, and extracellular vesicles. It makes up approximately 55% of the whole bone marrow suspension. This whole bone marrow plasma is isolated from a single donor. Briefly, the plasma is separated out from the whole bone marrow by centrifugation (2,000 g for 20 mins at room temperature) in anticoagulant (EDTA) coated vials. The upper, lighter yellowish layer, which is the plasma, is collected and immediately frozen at -80°C in order to preserve its contents. We instead used the term "bone marrow conditioned media" when the entire bone marrow cellular populations were cultured in exosome-free media and the supernatant was collected after 48 hrs of culture.

Animal models

Mice were housed under a 12 hour light-dark cycle with food and water ad libitum. miR-15a/16-1$^{-/-}$ mice (C57BL/6 background) were a generous gift from R. Dalla-Favera (Columbia University) (21). Monocytes/MΦ were isolated using the CD11b microbeads isolation kit (Cat# 130-049-601, Miltenyi Biotech, Bergisch Gladbach, Germany).

Isolation and ex vivo treatment of mouse spleen MΦ

Spleenocytes were isolated from healthy C57BL/6 wild type or miR-*15a*/*16-1* KO mice (21), and M0 MΦ were isolated using anti-mouse F4/80 MicroBeads isolation kit (Cat# 130-110-443, Miltenyi Biotech, Bergisch Gladbach, Germany) according to the manufacturer's instructions. F4/80 positive cells were cultured ex vivo at a density of 1x10^6 cells/ml in DMEM/F12-10 supplemented with 10% fetal bovine serum and 100 U/ml of recombinant murine M-CSF (Cat# 315-02, PeproTech) and incubated at 37°C with 5% CO_2. To induce MΦ differentiation to the M2 phenotype, at 8 hrs after isolation, 20 ng/ml of murine IL-4 was added and replenished every 2 days. Cells were harvested at both 48 hrs and 6 days of culture for detection of CD206 and Dectin-1 surface markers by flow cytometry (See flow cytometry section).

Extracellular vesicle isolation

The method used for isolation of cell line derived extracellular vesicles (EVs) was previously described by Thery et al (55). In short, serum-starved cells and media were centrifuged at 300 × g for 10 min at 4°C. Supernatant was collected and centrifuged again at 2000 × g for 20 min at 4°C. The cell pellets were frozen and stored at −80°C for later use. Supernatant was harvested and vacuum ultracentrifuged at 10 000 × g for 30 min at 4°C to remove residual cell debris. Supernatant was collected and ultracentrifuged at 100 000 × g for 70 min at 4°C under vacuum. The resulting supernatant was discarded. Pellets from multiple tubes were resuspended in 1 mL of PBS, pooled into a single tube, and ultracentrifuged at 100 000 ×g as described previously

(45). Supernatant was eliminated, and pellets of vesicles were resuspended in the desired amount of PBS and used for monocytes treatment (see section on monocyte differentiation).

miRNA microarray analysis

Intracellular or EV miRNA levels were measured as previously described (26). Briefly, 1 µg RNA isolated from cells or EVs released by cells was analyzed by NanoString assay performed as described by the manufacturer (NanoString Technologies, Inc, Seattle, Washington, USA). NanoString raw data, which were proportional to copy number, were log-transformed and normalized by the quantile method. P-values were used to rank miRNAs of interest, and correction for multiple comparisons was done using the Benjamini-Hochberg method.

DNA constructs

A trimer of wild type human NFκB binding site (wt3xtNFκB) and a trimer of human mutated NFκB binding site in pGL3 luciferase vectors were a generous gift from Dr. Denis Guttridge (The Ohio State University). For generation of a human 3'UTR IKKβ luciferase reporter construct containing a miR-16-5p wild type binding site, 249 base pairs were amplified and cloned into the XbaI site of pGL4.11 luciferase construct (Promega) using the following primers: (Forward) 5' ATCTAGATCCCTGTCCTCTCTCACTTTAC 3'
and (Reverse) 5' ATCTGAGGCTCTCCCATCCTGGTTACTAT 3'

A mutated 3'UTR IKKβ construct was generated by mutating the miR-16-5p binding site using QuikChange Site-Directed Mutagenesis Kit (Agilent Technologies) according to the manufacturer's instructions and the following primers:

(Forward) 5' CTTCCTCTTTTTATTTCACTGGATCCAAAATTGTGTTTTTACCTAC 3'

(Reverse) 5' GTAGGTAAAAACACAATTTTGGATCCAGTGAAATAAAAAGAGGAAG 3'

Mutations involve introduction of the Bam HI sites underlined above.

Statistics

All quantitative data were presented when indicated as the mean ± standard deviation, and at least three experiments were performed. GraphPad Prism 8 was used for data analysis. Experimental data with a normal distribution between two comparison groups were analyzed by unpaired T test (tails = 2). One-way ANOVA test was used to analyze experiments with multiple comparisons (>2 groups). The post-test value is reported for each analysis.

Study approval

All animal studies were approved by the City of Hope Institutional Laboratory Animal Care and Use Committee (IACUC). Our studies involving human subjects (NCT01408225) were approved by the Institutional Review Board of The Ohio State University or City of Hope and conformed to the tenets of the Declaration of Helsinki. Participants provided informed written consent.

Author contributions

JK performed experiments, analyzed the data and wrote the manuscript.

JG, MM, DV, ET, EGG performed experiments.

CT, **AS** analyzed the single cell flow cytometry data.

AR performed experiments and revised the manuscript.

PLB, MC, SR, GM, CCH, AK scientifically contributed to the experimental design and revised the manuscript

AP, JJK performed bioinformatics analyses.

AD helped prepare and design the figures

JFS scientifically corrected the manuscript.

EC performed experiments and helped supervise the project.

FP designed, directed the project and wrote the manuscript

Acknowledgments

Research was in part supported by the National Institutes of Health under grant number NIH-2-R01-CA201382 (CCH, FP) and by the MMORE for Multiple Myeloma Research Fund. We thank Mr. Robert Weingart and Dr. Ramasamy Santhanam for their support in accomplishing the experimental work. We also thank Dr. R. Dalla-Favera for providing us with the miR-15a/16-1$^{-/-}$ knockout mouse model and Dr. Irene Ghobrial for providing us with the MM.1S GFP/Luc+ cell line. We thank The Ohio State University Leukemia Tissue Bank (NCT01408225) for primary samples collection under the supervision of Dr. Craig C Hofmeister. We thank Wei Chen and Xiwei Wu at the City of Hope integrative genomics core for bioinformatics support. We would like also to thank Dr. Lucy Ghoda and Tinisha McDonald for primary sample collection from City of Hope Leukemia Tissue Bank. We recognize Elizabeth Hartman, Evelyn Flores, and Debbie Flood for administrative support. Research reported in this publication included work performed at the City of Hope Liquid Tissue Bank, Analytical Cytometry, and Integrative Genomics and Bioinformatics shared resource cores supported by the National Institutes of Health under award number P30CA033572. The content is solely the responsibility of the authors and does not necessarily represent the official views of the National Institutes of Health.

References

1. National Cancer Institute. Surveillance, Epidemiology, and End Results (SEER) Program and the National Center for Health Statistics. https://seer.cancer.gov/faststats/. Accessed September 19, 2018.
2. Fonseca R, and San Miguel J. Prognostic factors and staging in multiple myeloma. *Hematol Oncol Clin North Am.* 2007;21(6):1115-40, ix.
3. Fonseca R, et al. International Myeloma Working Group molecular classification of multiple myeloma: spotlight review. *Leukemia.* 2009;23(12):2210-21.
4. Weiss BM, Abadie J, Verma P, Howard RS, and Kuehl WM. A monoclonal gammopathy precedes multiple myeloma in most patients. *Blood.* 2009;113(22):5418-22.
5. Weiss BM, et al. Patterns of monoclonal immunoglobulins and serum free light chains are significantly different in black compared to white monoclonal gammopathy of undetermined significance (MGUS) patients. *Am J Hematol.* 2011;86(6):475-8.

6. Weiss BM, and Kuehl WM. Advances in understanding monoclonal gammopathy of undetermined significance as a precursor of multiple myeloma. *Expert Rev Hematol.* 2010;3(2):165-74.
7. Landgren O, and Rajkumar SV. Development of early treatment strategies for high-risk myeloma precursor disease in the future. *Semin Hematol.* 2011;48(1):66-72.
8. Kim J, et al. Macrophages and mesenchymal stromal cells support survival and proliferation of multiple myeloma cells. *Br J Haematol.* 2012;158(3):336-46.
9. Bianchi G, Richardson PG, and Anderson KC. Promising therapies in multiple myeloma. *Blood.* 2015;126(3):300-10.
10. Di Marzo L, et al. Microenvironment drug resistance in multiple myeloma: emerging new players. *Oncotarget.* 2016;7(37):60698-711.
11. Markovina S, et al. Bortezomib-resistant nuclear factor-kappaB activity in multiple myeloma cells. *Mol Cancer Res.* 2008;6(8):1356-64.
12. Demchenko YN, Glebov OK, Zingone A, Keats JJ, Bergsagel PL, and Kuehl WM. Classical and/or alternative NF-kappaB pathway activation in multiple myeloma. *Blood.* 2010;115(17):3541-52.
13. Keats JJ, et al. Promiscuous mutations activate the noncanonical NF-kappaB pathway in multiple myeloma. *Cancer cell.* 2007;12(2):131-44.
14. Demchenko YN, and Kuehl WM. A critical role for the NFkB pathway in multiple myeloma. *Oncotarget.* 2010;1(1):59-68.
15. Calin GA, et al. Frequent deletions and down-regulation of micro- RNA genes miR15 and miR16 at 13q14 in chronic lymphocytic leukemia. *Proc Natl Acad Sci U S A.* 2002;99(24):15524-9.
16. Zojer N, et al. Deletion of 13q14 remains an independent adverse prognostic variable in multiple myeloma despite its frequent detection by interphase fluorescence in situ hybridization. *Blood.* 2000;95(6):1925-30.
17. Shaughnessy J, et al. High incidence of chromosome 13 deletion in multiple myeloma detected by multiprobe interphase FISH. *Blood.* 2000;96(4):1505-11.
18. Lopez-Corral L, et al. The progression from MGUS to smoldering myeloma and eventually to multiple myeloma involves a clonal expansion of genetically abnormal plasma cells. *Clin Cancer Res.* 2011;17(7):1692-700.
19. Binder M, et al. Prognostic implications of abnormalities of chromosome 13 and the presence of multiple cytogenetic high-risk abnormalities in newly diagnosed multiple myeloma. *Blood cancer journal.* 2017;7(9):e600.
20. Avet-Loiseau H, et al. Monosomy 13 is associated with the transition of monoclonal gammopathy of undetermined significance to multiple myeloma. Intergroupe Francophone du Myelome. *Blood.* 1999;94(8):2583-9.
21. Klein U, et al. The DLEU2/miR-15a/16-1 cluster controls B cell proliferation and its deletion leads to chronic lymphocytic leukemia. *Cancer cell.* 2010;17(1):28-40.
22. Cimmino A, et al. miR-15 and miR-16 induce apoptosis by targeting BCL2. *Proc Natl Acad Sci U S A.* 2005;102(39):13944-9.
23. Liu J, et al. Loss of p53 and altered miR15-a/16-1short right arrowMCL-1 pathway in CLL: insights from TCL1-Tg:p53(-/-) mouse model and primary human leukemia cells. *Leukemia.* 2014;28(1):118-28.
24. Roccaro AM, et al. BM mesenchymal stromal cell-derived exosomes facilitate multiple myeloma progression. *The Journal of clinical investigation.* 2013;123(4):1542-55.
25. Lee JK, et al. Exosomes derived from mesenchymal stem cells suppress angiogenesis by down-regulating VEGF expression in breast cancer cells. *PLoS One.* 2013;8(12):e84256.
26. Rocci A, et al. Circulating miRNA markers show promise as new prognosticators for multiple myeloma. *Leukemia.* 2014;28(9):1922-6.

27. Jia X, et al. MiR-16 regulates mouse peritoneal macrophage polarization and affects T-cell activation. *Journal of cellular and molecular medicine.* 2016;20(10):1898-907.
28. Zheng Y, et al. Macrophages are an abundant component of myeloma microenvironment and protect myeloma cells from chemotherapy drug-induced apoptosis. *Blood.* 2009;114(17):3625-8.
29. Wang H, et al. High numbers of CD163+ tumor-associated macrophages correlate with poor prognosis in multiple myeloma patients receiving bortezomib-based regimens. *Journal of Cancer.* 2019;10(14):3239-45.
30. Baroni S, et al. Exosome-mediated delivery of miR-9 induces cancer-associated fibroblast-like properties in human breast fibroblasts. *Cell death & disease.* 2016;7(7):e2312.
31. Tang J, et al. Exosomal miR-9-3p suppresses HBGF-5 expression and is a functional biomarker in hepatocellular carcinoma. *Minerva medica.* 2018;109(1):15-23.
32. Roccaro AM, et al. MicroRNAs 15a and 16 regulate tumor proliferation in multiple myeloma. *Blood.* 2009;113(26):6669-80.
33. Manier S, Sacco A, Leleu X, Ghobrial IM, and Roccaro AM. Bone marrow microenvironment in multiple myeloma progression. *Journal of biomedicine & biotechnology.* 2012;2012:157496.
34. Beider K, et al. Multiple myeloma cells recruit tumor-supportive macrophages through the CXCR4/CXCL12 axis and promote their polarization toward the M2 phenotype. *Oncotarget.* 2014;5(22):11283-96.
35. Tran TH, Krishnan S, and Amiji MM. MicroRNA-223 Induced Repolarization of Peritoneal Macrophages Using CD44 Targeting Hyaluronic Acid Nanoparticles for Anti-Inflammatory Effects. *PLoS One.* 2016;11(5):e0152024.
36. Schmid JA, and Birbach A. IkappaB kinase beta (IKKbeta/IKK2/IKBKB)--a key molecule in signaling to the transcription factor NF-kappaB. *Cytokine Growth Factor Rev.* 2008;19(2):157-65.
37. Hagemann T, Biswas SK, Lawrence T, Sica A, and Lewis CE. Regulation of macrophage function in tumors: the multifaceted role of NF-kappaB. *Blood.* 2009;113(14):3139-46.
38. Sun SC. The noncanonical NF-kappaB pathway. *Immunol Rev.* 2012;246(1):125-40.
39. Agarwal V, Bell GW, Nam JW, and Bartel DP. Predicting effective microRNA target sites in mammalian mRNAs. *eLife.* 2015;4.
40. Chen ZJ. Ubiquitination in signaling to and activation of IKK. *Immunol Rev.* 2012;246(1):95-106.
41. Manni S, et al. Bone marrow stromal cell-fueled multiple myeloma growth and osteoclastogenesis are sustained by protein kinase CK2. *Leukemia.* 2014;28(10):2094-7.
42. Duluc D, et al. Interferon-gamma reverses the immunosuppressive and protumoral properties and prevents the generation of human tumor-associated macrophages. *Int J Cancer.* 2009;125(2):367-73.
43. De Beule N, et al. Tumour-associated macrophage-mediated survival of myeloma cells through STAT3 activation. *J Pathol.* 2017;241(4):534-46.
44. Kalluri R. The biology and function of exosomes in cancer. *J Clin Invest.* 2016;126(4):1208-15.
45. Harshman SW, et al. Characterization of multiple myeloma vesicles by label-free relative quantitation. *Proteomics.* 2013;13(20):3013-29.
46. Harshman SW, et al. Proteomic characterization of circulating extracellular vesicles identifies novel serum myeloma associated markers. *Journal of proteomics.* 2016;136:89-98.

47. Barkal AA, et al. Engagement of MHC class I by the inhibitory receptor LILRB1 suppresses macrophages and is a target of cancer immunotherapy. *Nat Immunol.* 2018;19(1):76-84.
48. Cheng Q, et al. Multiple Myeloma-Derived Exosomes Regulate the Functions of Mesenchymal Stem Cells Partially via Modulating miR-21 and miR-146a. *Stem cells international.* 2017;2017:9012152.
49. Manier S, et al. Prognostic role of circulating exosomal miRNAs in multiple myeloma. *Blood.* 2017;129(17):2429-36.
50. Hao M, et al. Suppressing miRNA-15a/-16 expression by interleukin-6 enhances drug-resistance in myeloma cells. *J Hematol Oncol.* 2011;4:37.
51. Li T, Morgan MJ, Choksi S, Zhang Y, Kim YS, and Liu ZG. MicroRNAs modulate the noncanonical transcription factor NF-kappaB pathway by regulating expression of the kinase IKKalpha during macrophage differentiation. *Nature immunology.* 2010;11(9):799-805.
52. Hagemann T, et al. "Re-educating" tumor-associated macrophages by targeting NF-kappaB. *J Exp Med.* 2008;205(6):1261-8.
53. Lovat F, et al. miR-15b/16-2 deletion promotes B-cell malignancies. *Proc Natl Acad Sci U S A.* 2015;112(37):11636-41.
54. Zhang L, et al. Potential role of exosome-associated microRNA panels and in vivo environment to predict drug resistance for patients with multiple myeloma. *Oncotarget.* 2016;7(21):30876-91.
55. Thery C, Amigorena S, Raposo G, and Clayton A. Isolation and characterization of exosomes from cell culture supernatants and biological fluids. *Curr Protoc Cell Biol.* 2006;Chapter 3:Unit 3 22.

Figures and figure legends

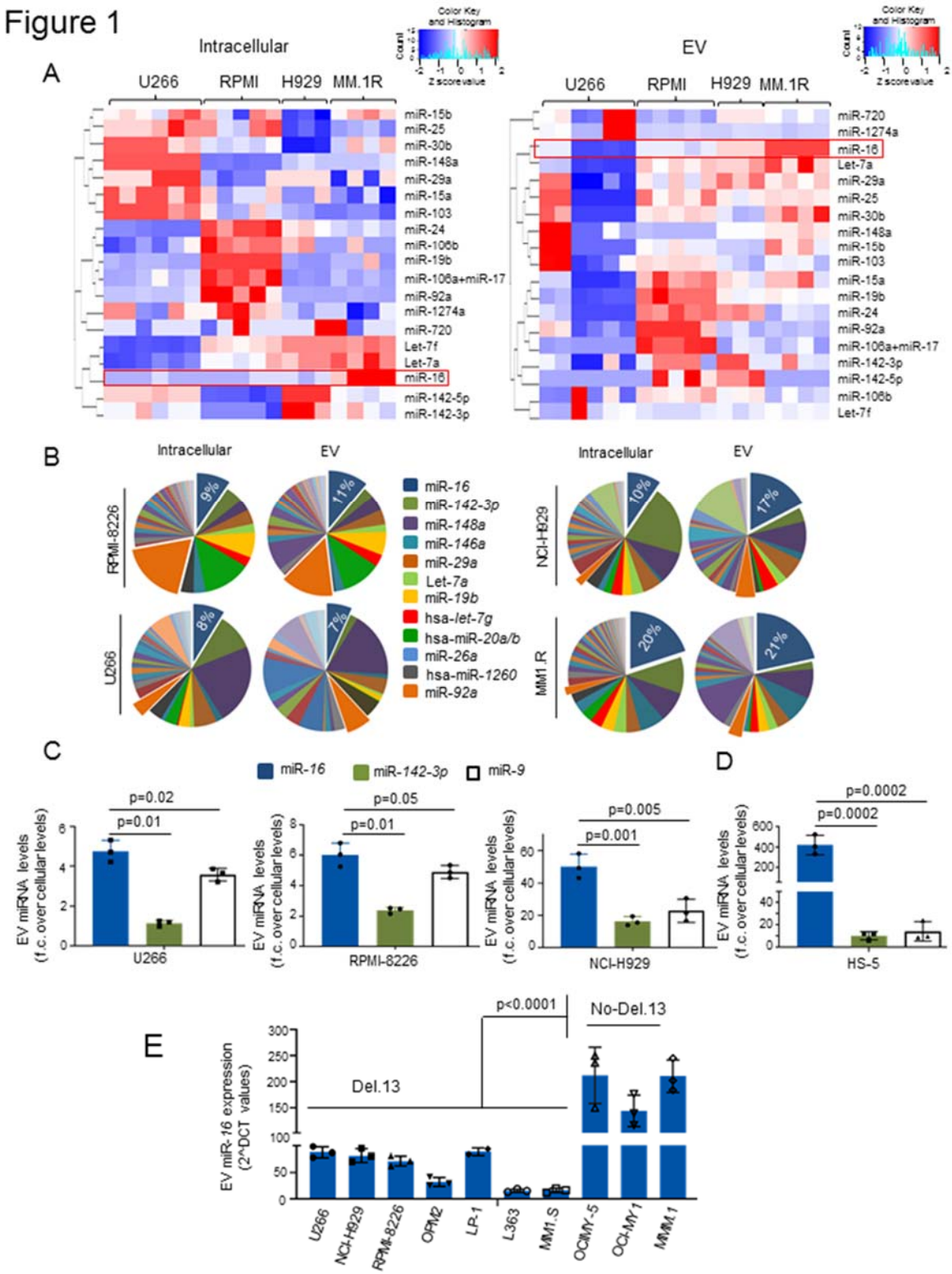

Figure 1. (A) Heatmaps showing microRNA expression profile as measured by the NanoString nCounter System in MM cells (RPMI-8226, U266, NCI-H929, MM1.R) (left panel) and in extracellular vesicles (EV) secreted by those cells (right panel). Each column represents one sample/cell line with red=upregulated, blue=downregulated. Each cell line was run at least in triplicate. Heatmaps were performed using the G-plots package heat map.2 program and colored scales generated using the Z score values. (B) Pie charts showing the percent of the 59 highest intracellular microRNA expression levels (left panel) and their corresponding EV secreted levels (right panel) in the four cell lines tested. The 12 highest microRNA expression levels among cell lines from miR-*16* (blue) to miR-*92a* (orange) are highlighted in a colored spectrum. (C) miR-*16,* miR-*142-3p* and miR-*9* expression levels in EVs released by U266, RPMI-8226 and NCI-H929 MM cell lines. Data are presented as fold change (f.c.) over intracellular microRNAs expression for each miRNA. (D) Parallel to (C) using HS-5 cell line. Values represent the mean ± SD; p values were calculated using ordinary one-way ANOVA multi comparisons test. Each experiment was performed in triplicate; (E) qRT-PCR showing miR-*16* expression in EVs released by Del(13) MM cell lines (U266, NCI-H929, RPMI-8226, OPM2, LP-1, L363, MM.1S) and non-Del(13) MM cell lines (OCIMY-5, OCIMY-I, MMM.1). Data are presented as $2^{\wedge -DCT}$ values. Values represent the mean ± SD; p values were calculated using t test unpaired (tails = 2). Each experiment was performed in triplicate the obtained p values are reported.

Figure 2

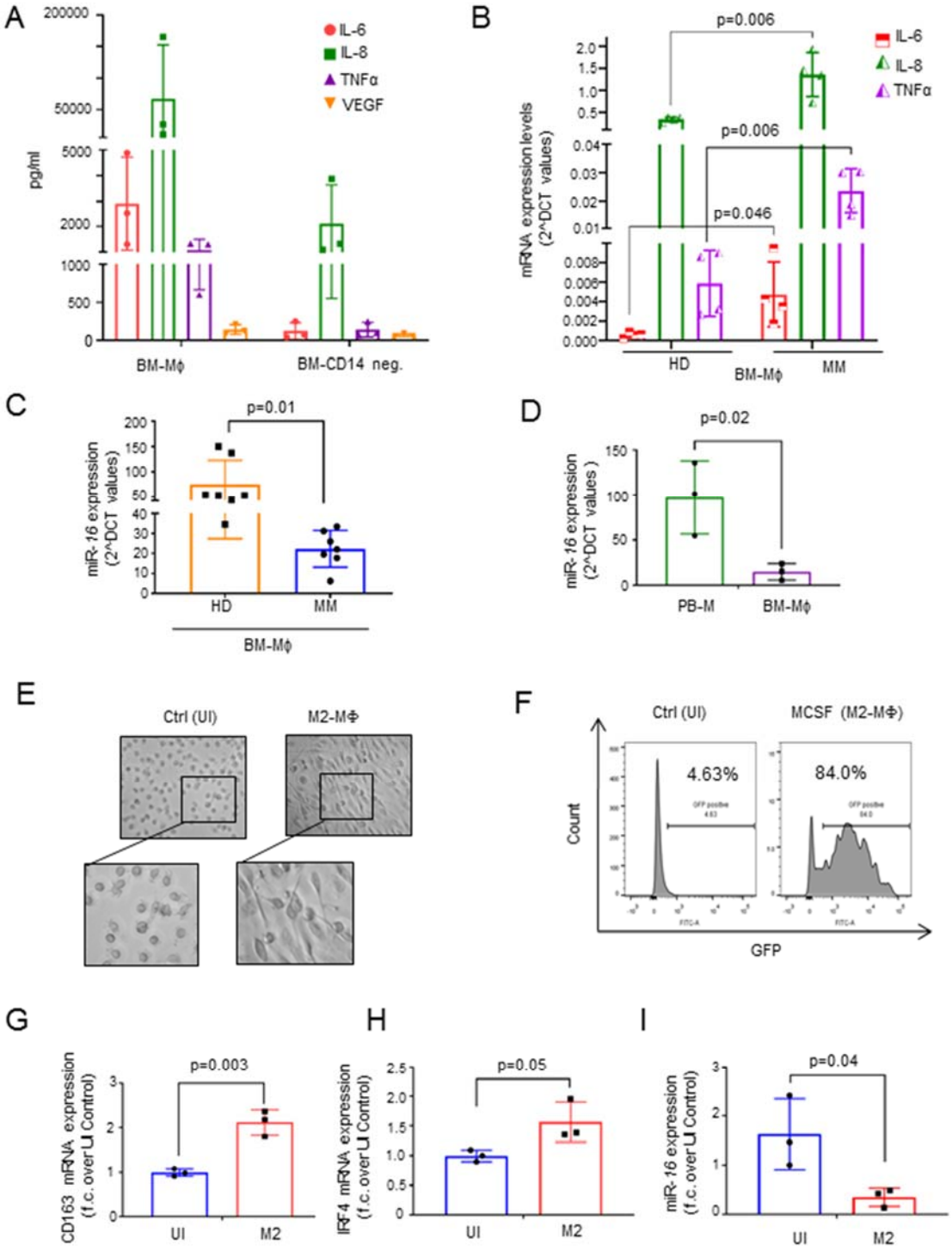
A
200000
50000
5000
2000
1000
500
0
pg/ml
IL-6
IL-8
TNFα
VEGF
BM-Mϕ
BM-CD14 neg.
B
p=0.006
p=0.006
p=0.046
IL-6
IL-8
TNFα
mRNA expression levels (2^DCT values)
HD
MM
BM-Mϕ
C
p=0.01
miR-16 expression (2^DCT values)
HD
MM
BM-Mϕ
D
p=0.02
miR-16 expression (2^DCT values)
PB-M
BM-Mϕ
E
Ctrl (UI)
M2-MΦ
F
Ctrl (UI)
MCSF (M2-MΦ)
4.63%
84.0%
Count
GFP
G
p=0.003
CD163 mRNA expression (f.c. over UI Control)
UI
M2
H
p=0.05
IRF4 mRNA expression (f.c. over UI Control)
UI
M2
I
p=0.04
miR-16 expression (f.c. over UI Control)
UI
M2

Figure 2. (A) Cytokine array showing, under stimulated conditions (i.e., in the presence of ssRNA-miR-25 which stimulates Toll-like receptors TLR-7 and -8), the levels of NF-κB-induced, M2-associated cytokines (IL-6, IL-8, TNFα and VEGF) secreted by CD14+ macrophages (BM-MΦ) and CD14- cells (BM-CD14 neg.) isolated from the BM of MM patients (n=3). Data represent mean values ± SD. Cells were incubated with ss miR-*25* for 24 hours prior to detection of cytokines. Cytokine levels were measured in pg/ml using a multiplex cytokine assay. (B) Quantitative RT-PCR showing mRNA expression levels of IL-6, IL-8 and TNF-α in BM-MΦ isolated from MM patients (MM) or cancer-free donors (HD) (n=4/group). P values were calculated using multiple T test (tails=2); (C) Quantitative RT-PCR showing decreased miR-*16* expression in BM-MΦ isolated from MM patients as compared to that isolated from HD (n= 7/group). (D) Real time PCR showing decreased expression of miR-*16* in BM-MΦ compared to that in monocytes isolated from the peripheral blood (PB-M) of the same MM patients (n=3). Data are presented as 2^-DCT values. (E) Representative images captured by light microscopy showing PB-M differentiated to M2-like MΦ (M2-MΦ) with macrophage colony stimulating factor (M-CSF) treatment for 7 days (right panel) as compared to undifferentiated PB-M (UI) (left panel). (F) Flow cytometric analysis showing phagocytosis of M2-MΦ *in vitro*. Phagocytosis assay was performed using latex beads coated with GFP fluorescent labeled IgG antibody. The engulfed fluorescent beads were detected by flow cytometry. Differentiated PB-M to M2-MΦ in the presence of M-CSF showed 84% GFP+ cells in contrast to UI cells that were only 4.63%.(G-H-I) Real time PCR showing increases in CD163 (G) and IRF4 (H) mRNA expression as well as a decrease in miR-*16* expression (I) in M2-MΦ as compared to UI. CD163 and IRF4 levels were presented as fold changes over UI controls. miR-*16* levels were presented as $2^{\wedge\text{-DCT}}$ values (n=3 patients). Data reported in C,D, G-I represent the mean ± SD; p values were calculated using an unpaired t test (tails = 2).

Figure 3

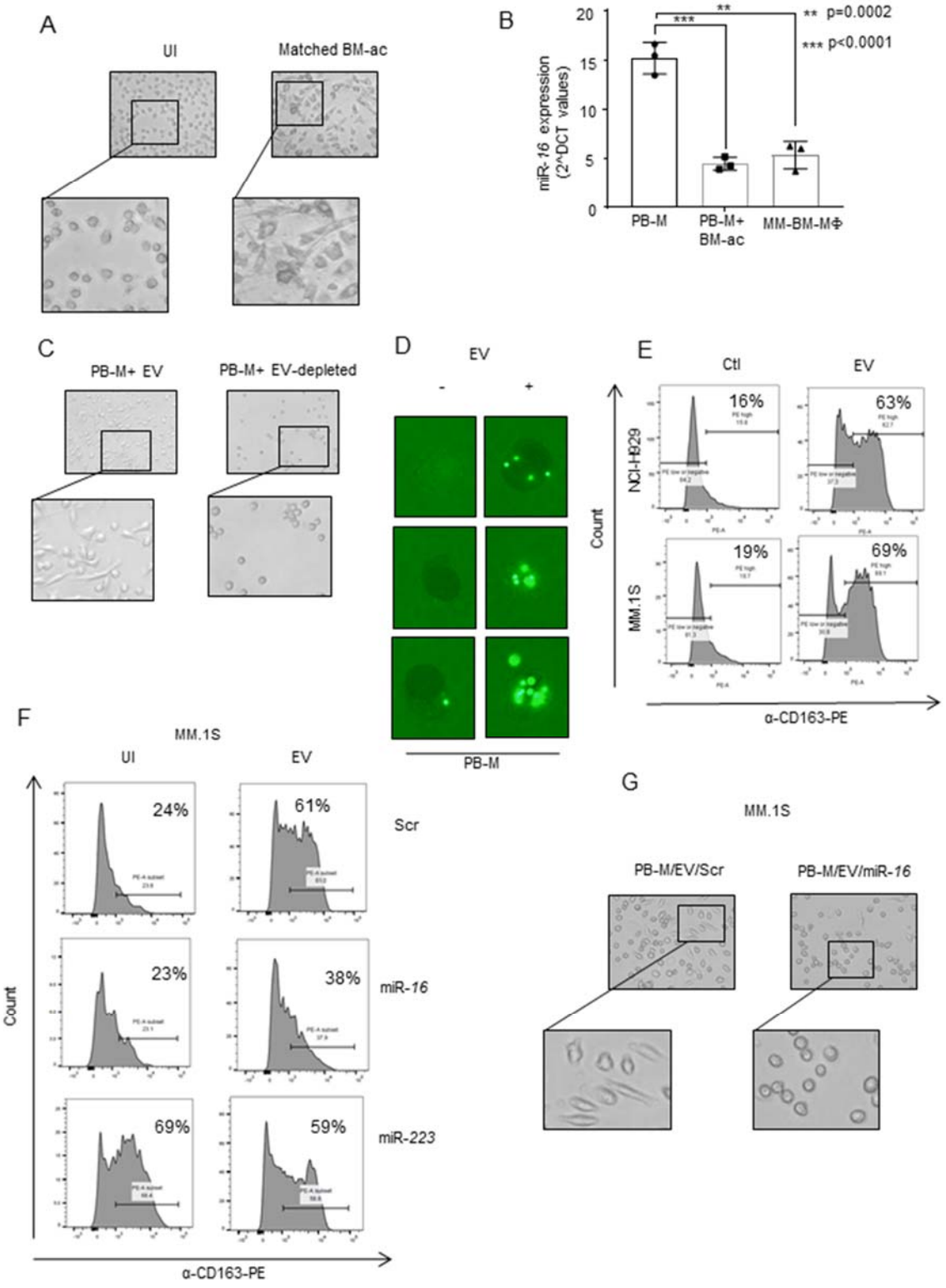
A
UI
Matched BM-ac
B
miR-16 expression (2^DCT values)
20
15
10
5
0
**
***
** p=0.0002
*** p<0.0001
PB-M
PB-M+ BM-ac
MM-BM-MΦ
C
PB-M+ EV
PB-M+ EV-depleted
D
EV
-
+
PB-M
E
Ctl
EV
NCI-H929
MM.1S
16%
63%
19%
69%
Count
α-CD163-PE
F
MM.1S
UI
EV
24%
61%
Scr
23%
38%
miR-16
69%
59%
miR-223
Count
α-CD163-PE
G
MM.1S
PB-M/EV/Scr
PB-M/EV/miR-16

Figure 3. (A) Representative images captured by light microscopy showing PB-M isolated from a MM patient differentiated to M2-MΦ in the presence of the matched BM acellular fraction (matched BM-ac) (right panel), in contrast to undifferentiated PB-M (UI) (left panel). (B) qRT-PCR showing decreased expression of miR-*16* in PB-M isolated from MM patient and differentiated to M2-MΦ in the presence of the matched BM acellular fraction (PB-M+BM-ac), as well as in total MΦ isolated from the BM of the same patient (MM-BM-MΦ), as compared to undifferentiated PB-M using samples obtained from n=3 MM patients. Values represent the mean ± SD; p values were calculated using ordinary one-way ANOVA multi-comparison. (C) Representative images captured by light microscopy showing differentiation of PB-M obtained from a HD incubated with EV isolated from the BM-acellular fraction of a MM patient (BM-ac) (left panel) or EV-depleted BM-ac (right panel) (n=4 patients; see Supplemental Figure 2B). (D) Representative images showing phagocytosis of latex beads coated with GFP-fluorescent labeled IgG antibody by PB-M differentiated to M2-MΦ when incubated with EV isolated from the BM-ac of a MM patient (+) (right panel), whereas no phagocytosis was observed when PB-M were incubated with the EV-depleted BM-ac (-) (left panel). The engulfed fluorescent beads were detected using a fluorescence microscope. (E) Flow cytometric analysis showing percent increase in expression of M2-MΦ surface marker (CD163) on PB-M treated with EV isolated from the conditioned media of a MM cell line, NCI-H929, for 7 days (EV) (upper right panel) and compared to cells incubated with EV-depleted acellular fraction (Ctl) (upper left panel). The same effect was seen using EV isolated from another MM cell line (MM.1S) (lower panel). Gating strategy was set using IgG anti-PE antibody isotype control. (F) Flow cytometric analysis showing percent surface expression of CD163 on PB-M differentiated with EV isolated from the conditioned media of MM.1S cells and concomitantly incubated with either ds-miR-*16* (middle right panel), ds-miR-*223* (lower right panel), or Scramble control (Scr) (upper right panel). CD163 percent surface expression on undifferentiated cells (UI) incubated with the microRNAs cited above are also shown (left panels).

Gating strategy was set using IgG anti-PE antibody isotype control. (G) Representative images captured by light microscopy showing impairment of PB-M differentiation to M2-MΦ in the presence of ds-miR-16. PB-M were incubated with the EV isolated from MM.1S along with ds miR-16 (right panel) or Scr control (left panel) for 7 days.

Figure 4

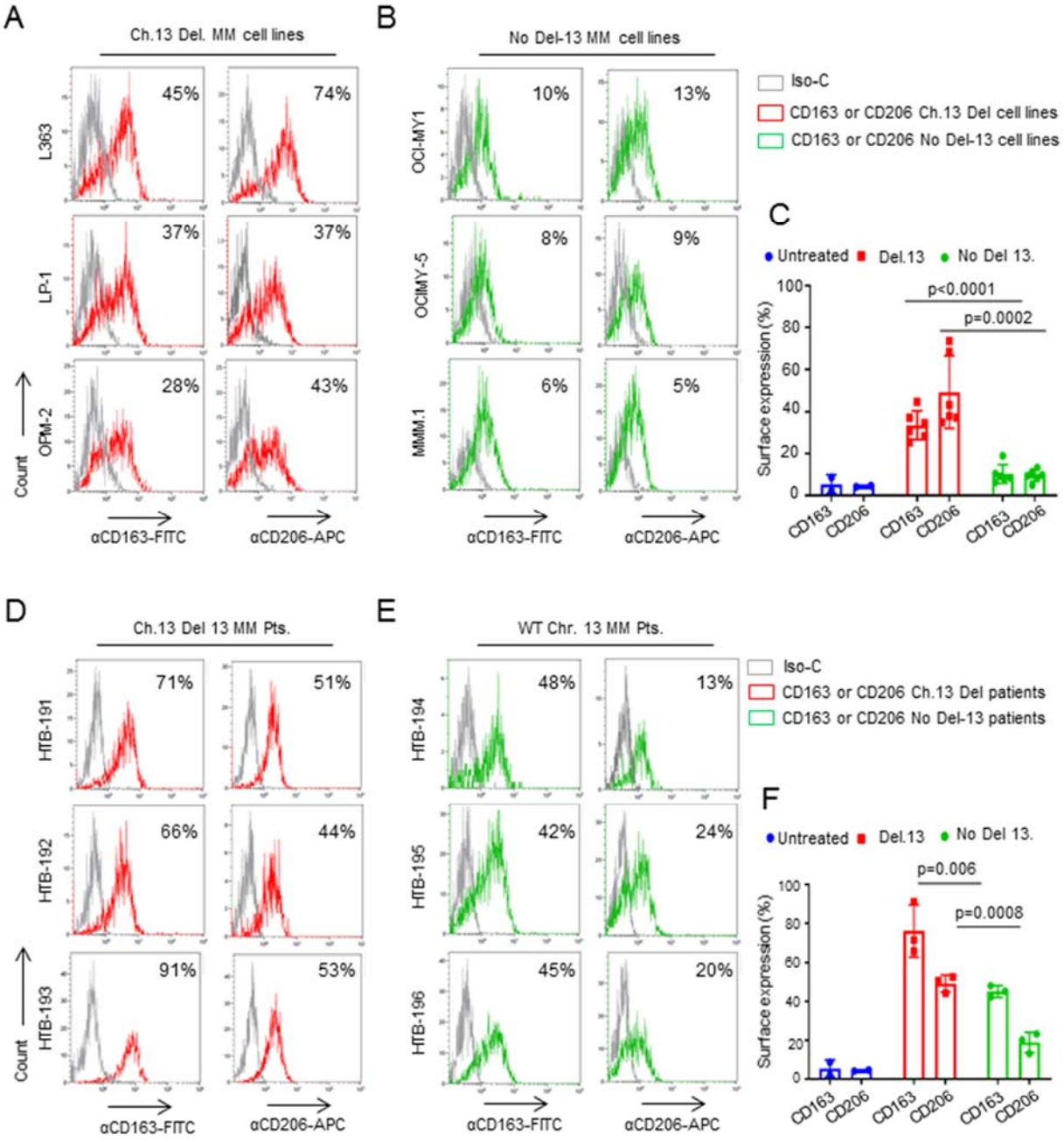
A
Ch.13 Del. MM cell lines
L363
LP-1
OPM-2
45%
74%
37%
37%
28%
43%
Count
αCD163-FITC
αCD206-APC
B
No Del-13 MM cell lines
OCI-MY1
OCIMY-5
MMM.1
10%
13%
8%
9%
6%
5%
αCD163-FITC
αCD206-APC
Iso-C
CD163 or CD206 Ch.13 Del cell lines
CD163 or CD206 No Del-13 cell lines
C
Untreated
Del.13
No Del 13.
p<0.0001
p=0.0002
Surface expression (%)
CD163
CD206
D
Ch.13 Del 13 MM Pts.
HTB-191
HTB-192
HTB-193
71%
51%
66%
44%
91%
53%
Count
αCD163-FITC
αCD206-APC
E
WT Chr. 13 MM Pts.
HTB-194
HTB-195
HTB-196
48%
13%
42%
24%
45%
20%
αCD163-FITC
αCD206-APC
Iso-C
CD163 or CD206 Ch.13 Del patients
CD163 or CD206 No Del-13 patients
F
Untreated
Del.13
No Del 13.
p=0.006
p=0.0008
Surface expression (%)
CD163
CD206

Figure 4 (A-B) Representative flowsight cytometric analysis overlaid with the respective Isotype control (Iso-C) showing comparable CD163 and CD206 percent surface expression on differentiated PB-M isolated from a healthy donor upon treatment with the EV isolated from Del(13) cell lines (L363, LP-1, OPM2) (A) or no Del(13) cells (OCIMY-5, OCIMY-I, MMM.1) (B) for 4 days. Gating strategy was set using a mix of IgG anti-FITC and IgG anti-APC antibodies isotype control (C) Bar dot plots showing average CD163 and CD206 percent surface expression on differentiated PB-M treated with EV-Del(13) cell lines (red diagrams n=3) or EV-no-Del(13) cell lines (green diagrams, n=3). Each dot plot represents a flowsight cytometric analysis percent reading. Statistical comparisons for each surface marker were performed only between Dell.13 and no Del(13) cell lines. Values represent the mean ± SD; p values were calculated using the unpaired t-test (tails = 2). Percent of untreated PB-M surface markers expression are indicated in blue diagrams and were only used as internal control. (D-E) Representative flowsight cytometric analysis overlaid with the respective Isotype control (Iso-C) showing comparable CD163 and CD206 percent surface expression on differentiated PB-M isolated from a healthy donor upon treatment with the BM-acellular fraction (BM-ac) of MM patients carrying Del(13) (HTB-191, HTB-192, HTB-193) (D) or BM-ac of MM patients with no Del(13) (HTB-194, HTB-195, HTB-196) (E) for 4 days. Gating strategy was set using a mix of IgG anti-FITC and IgG anti-APC antibody isotype controls. (F) Bar dot plots showing average CD163 and CD206 percent surface expression on differentiated PB-M treated with BM-ac of MM patients with Del(13) (red diagrams, n=3) or no-Del(13) (green diagrams, n=3). Percent of untreated PB-M surface markers expression are indicated in blue diagrams. Each dot plot represents a flowsight cytometric analysis percent reading. Statistical comparisons for each surface marker were performed only between Del(13) and no Del(13) patients. Values represent the mean ± SD; p values were calculated using t-test unpaired (tails = 2).

Figure 5

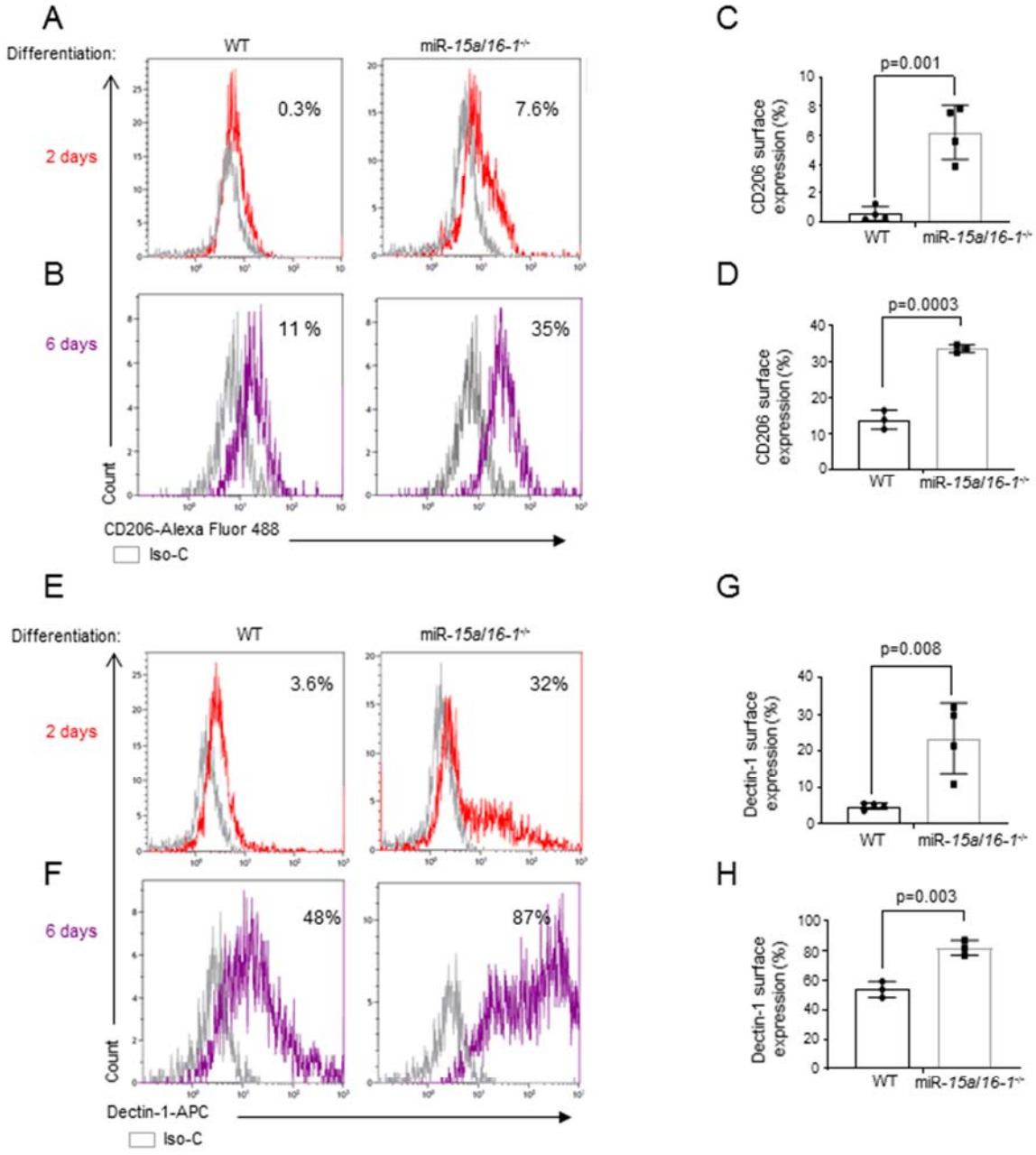
A
Differentiation:
WT
miR-15a/16-1-/-
2 days
0.3%
7.6%
B
6 days
11 %
35%
Count
CD206-Alexa Fluor 488
Iso-C
C
p=0.001
CD206 surface expression (%)
WT
miR-15a/16-1-/-
D
p=0.0003
CD206 surface expression (%)
WT
miR-15a/16-1-/-
E
Differentiation:
WT
miR-15a/16-1-/-
2 days
3.6%
32%
F
6 days
48%
87%
Count
Dectin-1-APC
Iso-C
G
p=0.008
Dectin-1 surface expression (%)
WT
miR-15a/16-1-/-
H
p=0.003
Dectin-1 surface expression (%)
WT
miR-15a/16-1-/-

Figure 5 (A-B) Representative flowsight cytometric analysis with overlaid isotype control (Iso-C) showing comparable CD206 percent surface expression on differentiated M0-MΦ isolated from WT or miR-*15a*/*16-1*$^{-/-}$ B6 mice spleens treated ex vivo with M-CSF (100 U/ml) and IL-4 (20 ng/ml) for 48 hrs (A) or 6 days (B). Gating strategy was set using an IgG anti-Alexa Fluor 488 antibody isotype control. (C-D) Bar dot plots showing average CD206 percent surface expression on differentiated MΦ isolated from WT and miR-*15a*/*16-1*$^{-/-}$ mice treated for 48 hrs (n=4 mice/group) (C) or 6 days (n=3 mice/group) (D). (E-F) is parallel to (A-B) except that the surface marker analyzed was Dectin-1 and the gating strategy was set using an IgG anti-APC antibody isotype control. (G-H) is parallel to (C-D) except that percents of Dectin-1 expression were recorded. Values represent the mean ± SD; p values were calculated using t-test unpaired (tails = 2) and the p values are reported in the figures.

Figure 6

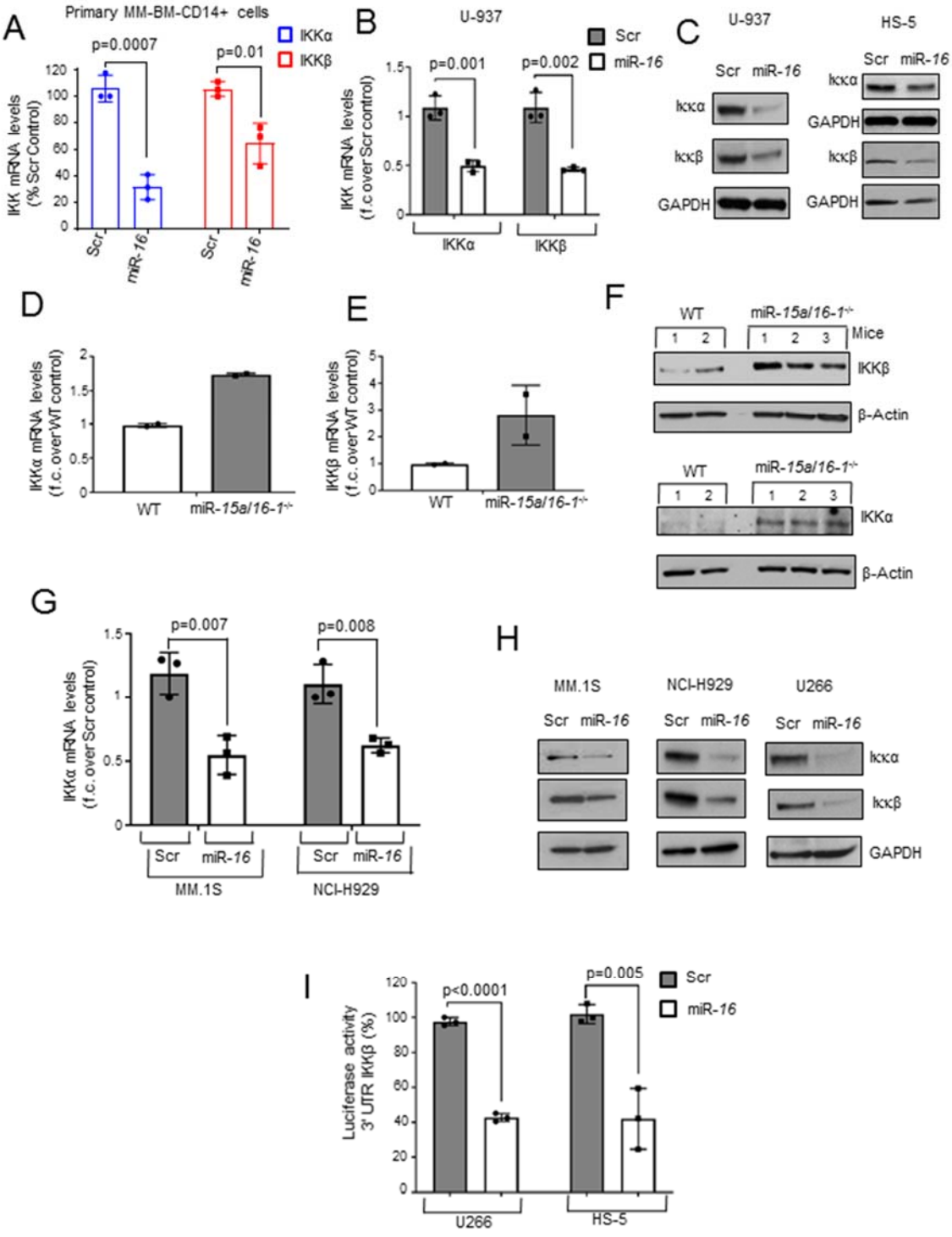
A
Primary MM-BM-CD14+ cells
IKKα
IKKβ
p=0.0007
p=0.01
IKK mRNA levels (% Scr Control)
Scr
miR-16
B
U-937
Scr
miR-16
p=0.001
p=0.002
IKK mRNA levels (f.c. over Scr control)
IKKα
IKKβ
C
U-937
HS-5
Scr miR-16
Scr miR-16
IκκαIκκβ
GAPDH
D
IKKα mRNA levels (f.c. over WT control)
WT
miR-15a/16-1-/-
E
IKKβ mRNA levels (f.c. over WT control)
WT
miR-15a/16-1-/-
F
WT
miR-15a/16-1-/-
1 2
1 2 3
Mice
IKKβ
β-Actin
WT
miR-15a/16-1-/-
1 2
1 2 3
IKKα
β-Actin
G
IKKα mRNA levels (f.c. over Scr control)
p=0.007
p=0.008
Scr miR-16
Scr miR-16
MM.1S
NCI-H929
H
MM.1S
NCI-H929
U266
Scr miR-16
Scr miR-16
Scr miR-16
IκκαIκκβ
GAPDH
I
Luciferase activity 3' UTR IKKβ (%)
p<0.0001
p=0.005
Scr
miR-16
U266
HS-5

Figure 6 (A-B) Real time PCR analysis revealing mRNA expression of IKKα and β complex in (A) MΦ isolated from MM patients (n=3) and (B) U-937 cell line, each transfected with ds miR-*16* or Scr control for 48 hrs. (C) Western blot analysis showing protein downregulation of IKKα and β by miR-*16* in U-937 (left panel) and HS-5 cells (right panel) as compared to Scr control after 48 hrs of treatment; GAPDH was used as loading control. (D-E) Real time PCR showing mRNA expression of IKKα (D) and β (E) in differentiated MΦ isolated from WT or miR-*15a*/*16-1*$^{-/-}$ mice spleens (n=4/group; the RNA from each two mice/group were pooled together for quality purposes and a triplicate PCR reading was done for each pool). In (D,E), error bars represent variance. (F) Western blot analysis showing protein levels of IKKβ and IKKα in monocytes/MΦ CD11b fractions isolated from wild type (WT) or miR-*15a*/*16-1*$^{-/-}$ mice spleens. (n=2 mice WT; n=3 mice miR-*15a*/*16-1*$^{-/-}$). β-Actin is used as loading control. (G) Real time PCR showing mRNA downregulation of IKKα expression in MM cell lines (MM.1S and NCI-H929) transfected with ds-miR-*16* as compared to Scr control for 48 hrs. (H) Western blot analysis showing protein downregulation of IKKα and β by miR-*16* in three MM cell lines (U266, MM.1S and NCI-H929); GAPDH is used as loading control. (I) Luciferase reporter assay revealed direct downregulation of IKKβ 3'UTR transcriptional activity by miR-*16*. pGL4.11 luciferase vector containing the 3'UTR of IKKβ was transfected in U266 or HS-5 for 18 hrs, followed by a second transfection with ds-miR-*16* or Scr control for an additional 12 hrs. Transfection efficiency was controlled by co-transfection with TK promoter-Renilla vector. Data are presented as percent of Scr control. When not otherwise specified in the legend the reported p values were calculated using unpaired t-test (tails = 2). Each of the reported experiment were performed in triplicate. For (C,H), the data presented are representative of two independent experiments.

Figure 7

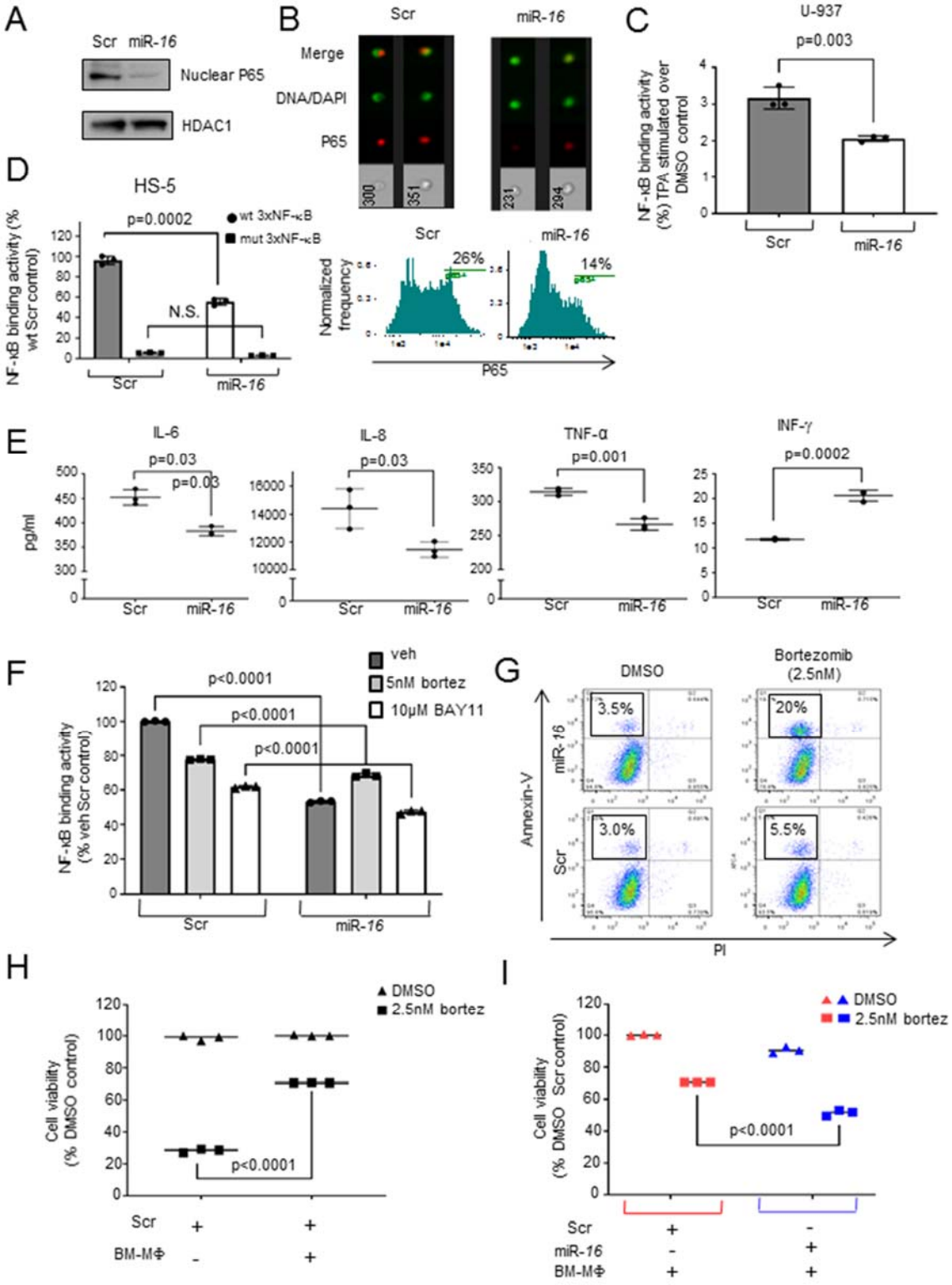
A
Scr miR-16
Nuclear P65
HDAC1
B
Scr
miR-16
Merge
DNA/DAPI
P65
300
351
231
294
C
U-937
p=0.003
NF-κB binding activity (%) TPA stimulated over DMSO control
Scr
miR-16
D
HS-5
p=0.0002
wt 3xNF-κB
mut 3xNF-κB
N.S.
NF-κB binding activity (% wt Scr control)
Scr
miR-16
Scr
miR-16
26%
14%
Normalized frequency
P65
E
IL-6
p=0.03
p=0.03
IL-8
p=0.03
TNF-α
p=0.001
INF-γ
p=0.0002
pg/ml
Scr
miR-16
F
veh
5nM bortez
10μM BAY11
p<0.0001
p<0.0001
p<0.0001
NF-κB binding activity (% veh Scr control)
Scr
miR-16
G
DMSO
Bortezomib (2.5nM)
Annexin-V
miR-16
Scr
3.5%
20%
3.0%
5.5%
PI
H
DMSO
2.5nM bortez
Cell viability (% DMSO control)
p<0.0001
Scr
BM-MΦ
I
DMSO
2.5nM bortez
Cell viability (% DMSO Scr control)
p<0.0001
Scr
miR-16
BM-MΦ

Figure 7 (A) Western blot analysis showing decrease in P65 nuclear protein in NCI-H929 upon transfection with ds-miR-*16* or Scr Control for 48h. Histone Deacetylase 1 (HDAC1) was used as nuclear loading control. (B) Single cell flow cytometric analysis showing decrease in nuclear p65 protein expression in MM cells upon transfection with ds-miR-*16* as compared to Scr control (upper panel). Percent of normalized P65 frequency in 10^4 cells transfected with ds-miR-*16* or Scr control are shown (lower panel). (C) Luciferase reporter assay showing decrease in NF-κB transcriptional activity in U-937 cells by miR-*16* as compared to Scr Control. (D) Parallel to (C) except that luciferase activity was assessed in HS-5 cells, no stimulation was induced, and an additional transfection with pGL3 vector containing a trimer of mutated NF-κB binding sites sequence (mut 3xNFκB) was performed. Data are presented as percent of wt 3xNFκB Scr control. (E) Cytokine array showing concentrations of cytokines/chemokines IL-6, IL-8, TNF-α and INF-γ released by BM-MΦ isolated from MM patient upon treatment with ds-miR-*16* or Scr sequences encapsulated in liposomes for 48 hrs. (F) Luciferase reporter assay showing decrease in NF-κB transcriptional activity in U266 upon transfection with miR-*16* as compared to Scr control. Cells were transfected with pGL3 luciferase vector containing a trimer of consensus wild type NF-κB binding sites for 6h, then treated with 5 nM bortezomib (bortez), 10 μM BAY11-7082, or vehicle control (veh) for 12h. Data are presented as percent of Scr veh control. Ordinary one-way ANOVA test was used for the reported p value calculations. (G) Representative flowsight showing apoptosis analysis by Annexin-V/PI double staining. Annexin-V/PI staining was performed on MM.1S cells upon transfection with miR-*16* or Scr sequences and treated with bortezomib 2.5 nM or veh DMSO control for 48 hrs. The percentages of Annexin-V-positive cells are shown in the upper left quadrants. (H) Luciferase assay showing percent of viable MM.1S GFP/Luc$^+$ cells in suspension upon treatment with bortezomib or DMSO veh control, co-cultured with BM-MΦ isolated from a patient for 48 hrs. Data are percent of DMSO veh control. (I) Luciferase assay showing percentage of viable MM.1S GFP/Luc$^+$ cells in suspension upon treatment with

bortezomib or DMSO veh control co-cultured with BM-MΦ isolated from a MM patient and treated with ds-miR-*16* or Scr sequences for 48 hrs. Data are percent of DMSO Scr control. Values represent the mean ± SD for each experiment performed in triplicate. When not otherwise specified in the legend the reported p values were calculated using unpaired t-test (tails = 2).

Figure 8

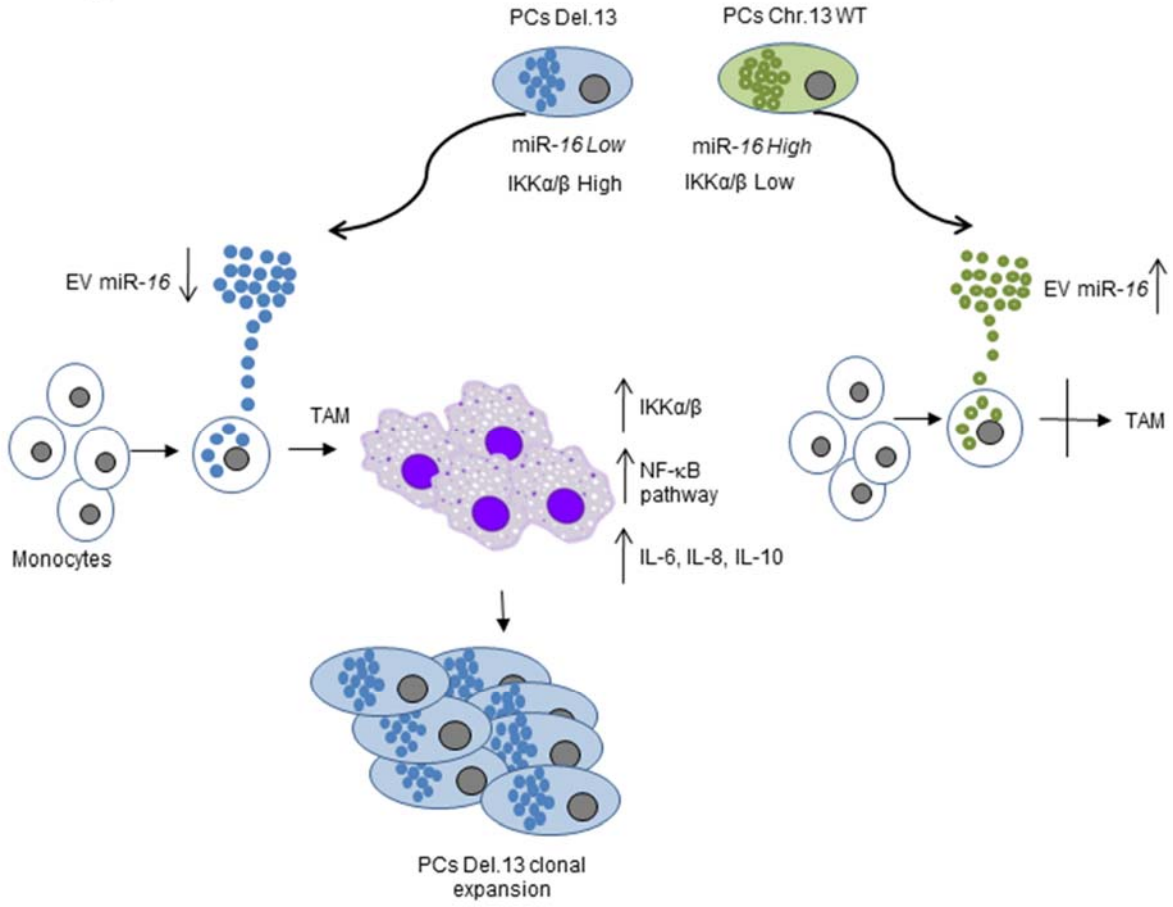

Figure 8 Illustrative diagram showing plasma cells carrying Del(13) (PCs Del(13)) secrete extracellular vesicles (EV) containing cargoes that induce monocyte differentiation toward M2 tumor-supporting MΦ (TAM). Mechanistically, a lack of significant amounts of miR-*16* in EV prevents targeting the IKKα/β complex, resulting in an increase in the NF-κB canonical pathway. Upregulation of the NF-κB pathway leads to enhanced secretion of M2 tumor effector chemokines/cytokines including IL-6, IL-8, IL-10, and TNF-α, resulting in an increase in TAM levels and in PC clonal expansion. However, normal PCs or PCs carrying wild type chromosome 13 (PCs Chr.13 WT) have higher levels of miR-*16* in their EV that target the IKKα/β complex,

resulting in a decrease in the NF-κB canonical pathway and impairment of monocyte differentiation towards the M2-MΦ subset of the microenvironment and thus PC clonal expansion.